LETTERS

Demonstration of controlled-NOT quantum gates on a pair of superconducting quantum bits

J. H. Plantenberg[1], P. C. de Groot[1], C. J. P. M. Harmans[1] & J. E. Mooij[1]

Quantum computation requires quantum logic gates that use the interaction within pairs of quantum bits (qubits) to perform conditional operations[1]. Superconducting qubits may offer an attractive route towards scalable quantum computing. In previous experiments on coupled superconducting qubits, conditional gate behaviour[2] and entanglement[3] were demonstrated. Here we demonstrate selective execution of the complete set of four different controlled-NOT (CNOT) quantum logic gates, by applying microwave pulses of appropriate frequency to a single pair of coupled flux qubits. All two-qubit computational basis states and their superpositions are used as input, while two independent single-shot SQUID detectors measure the output state, including qubit–qubit correlations. We determined the gate's truth table by directly measuring the state transfer amplitudes and by acquiring the relevant quantum phase shift using a Ramsey-like interference experiment. The four conditional gates result from the symmetry of the qubits in the pair: either qubit can assume the role of control or target, and the gate action can be conditioned on either the 0-state or the 1-state. These gates are now sufficiently characterized to be used in quantum algorithms, and together form an efficient set of versatile building blocks.

In order to use superconducting circuits in quantum computing implementations, it is necessary to find a way to implement efficient quantum logic gates on pairs of qubits. Single superconducting qubits can be designed to operate in the charge[4], charge-phase[5], flux[6] and phase[7] regimes. In our experiments, we use a flux qubit consisting of a superconducting loop interrupted by three Josephson junctions, which can behave as a quantum two-level system[8]. Varying the magnetic flux threading the loop controls the energy level separation. At exactly half a flux quantum, the two classical states carrying a clockwise and an anticlockwise persistent current are degenerate. Quantum mechanical level repulsion occurs, and the eigenstates are formed by a symmetric and an antisymmetric superposition of the classical current states. When moving away from the degeneracy point, the eigenstates approach the classical current states and produce a net magnetic field. The qubit state is manipulated using microwave pulses resonant with the level separation; the circulating currents are used to detect the state with a superconducting quantum interference device (SQUID) magnetometer.

Previously, in experiments on two interacting superconducting qubits, spectroscopy was demonstrated[9–12] as well as coherent qubit–qubit interaction controlled by non-adiabatic bias shifts[2,3,13,14]. In our experiments, we couple two flux qubits magnetically with a fixed strength, resulting in a four-level system that is tunable with the individual flux biases. Four different two-qubit operations are realized with simple microwave pulses. The sample is depicted in Fig. 1. The qubit pair is described by the hamiltonian

$$H = H_1 + H_2 + H_{12} = -\tfrac{1}{2}\left(\varepsilon_1\sigma_z^1 + \Delta_1\sigma_x^1 + \varepsilon_2\sigma_z^2 + \Delta_2\sigma_x^2\right) + J\sigma_z^1\sigma_z^2 \quad (1)$$

where $\varepsilon_i = 2I_{\mathrm{p},i}(\Phi_i - \tfrac{1}{2}\Phi_0)$ represent the magnetic energy biases with $I_{\mathrm{p},i}$ the persistent currents, Φ_i the fluxes threading the loop and Φ_0 the superconducting flux quantum, Δ_i determine the coupling between the two classical current states of the single qubits, J is the qubit–qubit coupling energy and $\sigma_{x,y,z}^i$ are the Pauli spin matrices. To use the flux
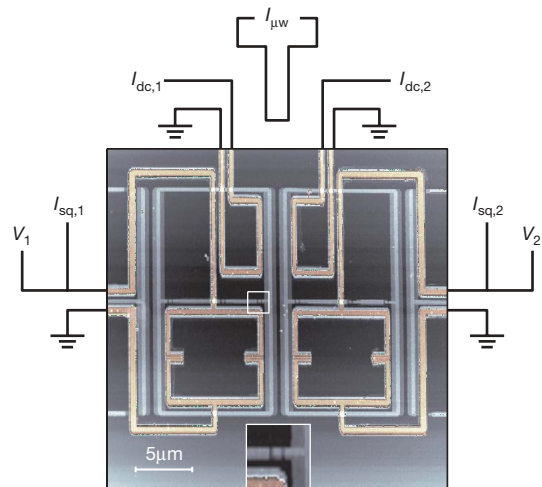

Figure 1 | Coupled-qubits set-up. Atomic force micrograph of the sample, showing the two '8'-shaped flux qubits in light grey. These are a gradiometric variety of the common three-junction flux qubit, using a trapped supercurrent in the outer uninterrupted loop to bias the qubit at its degeneracy point[18]. The three Josephson junctions defining the qubit are visible on the middle horizontal branches; a single junction (white box) is shown magnified in the inset. The qubits are fabricated with electron beam lithography and two-angle shadow evaporation of aluminium. Two junctions are characterized by the ratio of Josephson to charging energy, $E_J/E_C = 36$; the relative area of the third is taken to be $\alpha = 0.75$. The persistent currents $I_{\mathrm{p},i}$ and energy gaps Δ_i are 450 nA and $h \times 2.6$ GHz for the first qubit, and 480 nA and $h \times 2.2$ GHz for the second. In the presented experiments, the first qubit is chosen to act as control (C) and the second as target (T). The coupling strength $2J = h \times 400$ MHz. On top of the qubits, two SQUIDs (shown in orange), used as switching qubit-state detectors, are fabricated in a separate lithography step. They are electrically isolated from the qubits, and operated by carefully-timed sample-and-hold (5-ns and 250-ns) d.c. pulses from current sources $I_{\mathrm{sq},1}$ and $I_{\mathrm{sq},2}$ (ref. 6). The resulting voltages V_1 and V_2, which depend on the qubit state, are detected using amplifiers and threshold detectors. Currents $I_{\mathrm{dc},1}$ and $I_{\mathrm{dc},2}$ bias the qubits through two small coils (shown in orange); in the experiments the energy level separations are $\nu_C = 7$ GHz and $\nu_T = 5$ GHz, applying currents $I_{\mathrm{dc},i} \approx 10$ μA. Here the characteristic times are $T_1 = 50$–100 ns, $T_{2,\mathrm{free}} \approx 5$ ns and $T_{2,\mathrm{Rabi}} = 15$–20 ns. Qubit transitions are induced magnetically using an on-chip wire connected to a 50 Ω microwave source, $I_{\mu w}$. The experiments are performed in a dilution refrigerator at $T \approx 50$ mK, with all current and voltage connections carefully filtered and/or attenuated.

coupling effectively, the qubits are operated far from their degeneracy points, that is $\varepsilon_i > \Delta_i$, so the qubit energy separations are $v_i = \sqrt{\varepsilon_i^2 + \Delta_i^2} \approx \varepsilon_i$. As shown in Fig. 2a, this results in four resonance frequencies that change the state of either the first or second qubit. By way of the state-dependent circulating current, one qubit shifts the other's resonance frequency and vice versa. Consequently, all transitions are all either 0-controlled or 1-controlled operations, with 0 and 1 representing the state of the second qubit. Given the symmetry of the qubits in the pair, we are free to select either one to act as the control (C) qubit and the other as the target (T) qubit, thereby defining the computational basis 0_C0_T, 0_C1_T, 1_C0_T, 1_C1_T. A resonant microwave pulse induces rotations in this basis, and its microwave phase determines the orientation of the rotation axis (see Supplementary Information). The pulse induces a quantum gate, which is characterized by a transfer matrix relating input to output states, both in amplitude and phase. For example, a microwave pulse inducing a rotation around the x axis of the 1_C0_T–1_C1_T transition (and thus off-resonant with respect to the 0_C0_T–0_C1_T transition) is expressed by the gate matrix:

$$\hat{R}_{1_C0_T - 1_C1_T}(\omega, \tau) = \begin{pmatrix} 1 & 0 & 0 & 0 \\ 0 & 1 & 0 & 0 \\ 0 & 0 & \cos\frac{\omega\tau}{2} & i\sin\frac{\omega\tau}{2} \\ 0 & 0 & i\sin\frac{\omega\tau}{2} & \cos\frac{\omega\tau}{2} \end{pmatrix} \quad (2)$$

where τ is the pulse length and ω is the Rabi frequency. This conditional rotation performs the ideal CNOT gate if $\omega\tau = \pi$, up to a single-qubit quantum phase shift. Here we only show measurements for this 1_C-controlled excitation of the target qubit, corresponding to the usual CNOT gate. Similar results were obtained when the 0_C-controlled transition was induced (see Supplementary Information) and when control and target qubits were interchanged, yielding the four transitions of different frequency. Note that with this scheme one can conveniently produce the four maximally entangled two-particle Bell states, by applying two consecutive microwave pulses. Comparable techniques have been used in nuclear magnetic resonance experiments[15].

In Fig. 2d the microwave pulse scheme of the presented experiments is shown. The system is initialized by allowing it to relax to the ground state 0_C0_T, after which the desired input state is prepared. Now a two-qubit conditional gate is executed using a pulse selective to either a 0- or 1-controlled transition. Next, probe pulses can be applied to analyse the resulting density matrix. Finally, the states of the two qubits are determined simultaneously and independently using the two single-shot state detectors. Repeating this scheme N times, the result is represented by the state counts N_{00}, N_{01}, N_{10} and N_{11}, directly yielding the measured joint-probabilities P_{00}, P_{01}, P_{10} and P_{11}. In addition to the individual switching probabilities of the control and target qubit detectors, $P_C = P_{10} + P_{11}$ and $P_T = P_{01} + P_{11}$, this method extracts correlation information, $P_{C=T} = P_{00} + P_{11}$.

To determine the output amplitudes of the CNOT gate for input superpositions of 0_C0_T and 1_C0_T, the pulse sequence depicted in Fig. 2b is used. After its creation, this state is subjected to the gate pulse resonant with the 1_C0_T–1_C1_T transition. In Fig. 3a, the switching probability of the control qubit detector shows the superposition created by the first pulse. Figure 3c shows that when the 1_C-controlled gate pulse induces an odd number of π rotations it executes a CNOT gate, inverting the target qubit state only if the control qubit was in the state 1_C; for the 0_C state the gate pulse is off-resonant, leaving the target qubit unaffected. Similarly, Fig. 2c illustrates the pulse sequence used to determine the matrix amplitudes for input superpositions of 0_C1_T and 1_C1_T. First, the target qubit is initialized in the 1_T state by inducing a π rotation on the 0_C0_T–0_C1_T transition. The control qubit is then brought into a superposition by driving the 0_C1_T–1_C1_T transition, as depicted in Fig. 3b. Finally, the CNOT gate is executed with the identical microwave gate pulse as used previously for the 0_C0_T–1_C0_T superposition input states. Figure 3d shows that the gate only inverts the target qubit back to the state 0_T if the control qubit was in the state 1_C.

The truth table amplitudes follow directly from the joint-probabilities. In Fig. 4a the output state counts are depicted for the prepared computational basis input states. The measured data
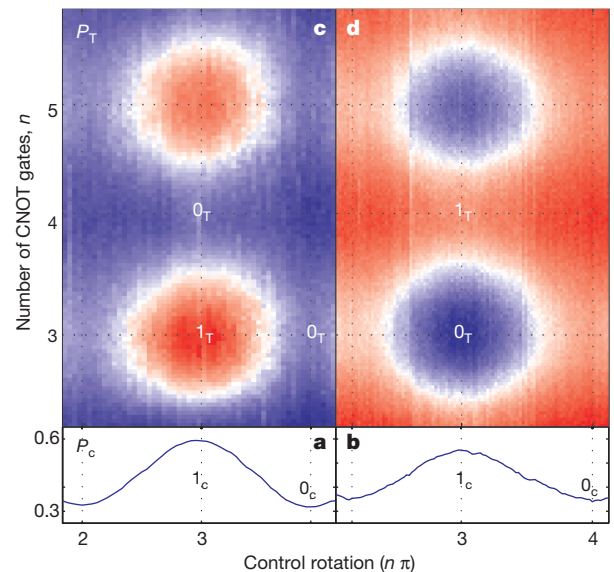
Figure 3 | 1_C-controlled gate operation. The horizontal axis represents the control qubit rotation, and the ordinate of the colour figures sets the number of CNOT gates (n) that was executed. The pulses needed for control and gate rotations significantly smaller than π were too short to generate reliably. **a, b,** Control qubit input state preparation, where P_C represents the measured switching probability of the control qubit detector. A 2π rotation corresponds to a pulse length of 5 ns. **c, d,** Target qubit state after the CNOT pulse, where P_T represents the measured switching probability of the target qubit detector, ranging from 0.3 (blue) through 0.5 (white) to 0.7 (red). A single CNOT π rotation corresponds to a 3 ns pulse. **a, c,** Results for superpositions of the 0_C0_T and 1_C0_T input states, corresponding to the experimental scheme of Fig. 2b. **b, d,** Results for superpositions of the 0_C1_T and 1_C1_T input states, corresponding to the experimental scheme of Fig. 2c.
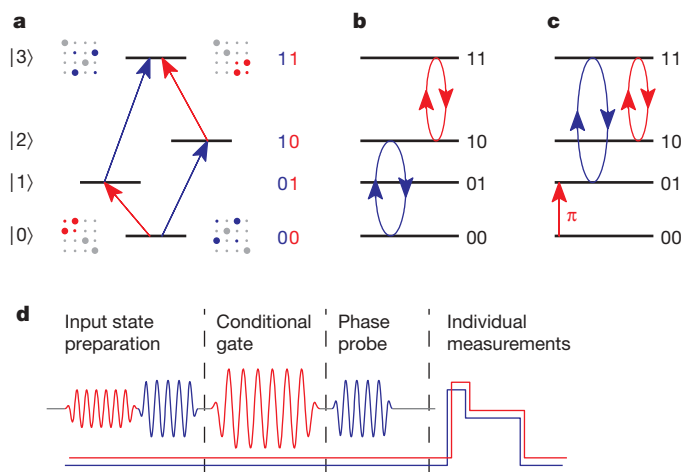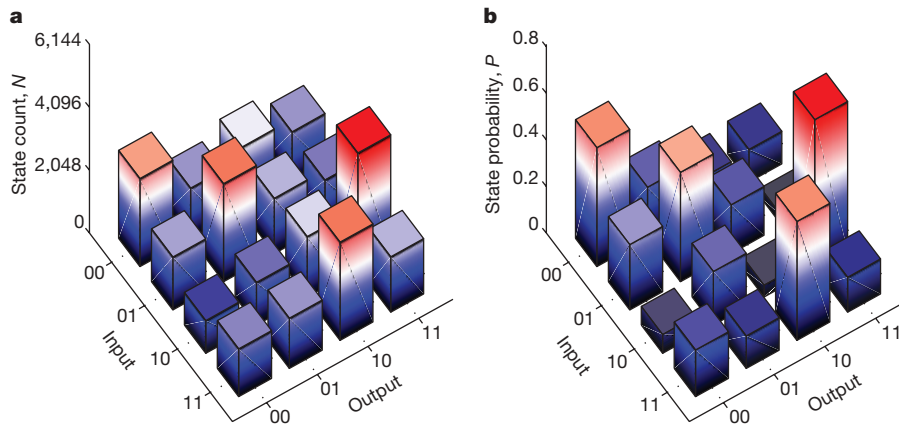

Figure 2 | Operation of the coupled-qubits device. a, Energy level diagram of the two-qubit system. The qubit transitions are indicated by blue and red arrows, and the corresponding rotation matrices are depicted schematically with the computational basis increasing from left to right and from top to bottom. **b,** Sequence of operations to determine the truth table amplitudes for superpositions of the 0_C0_T and 1_C0_T input states. **c,** As **b** but for superpositions of the 0_C1_T and 1_C1_T input states. The π pulse initializes the target qubit in the state 1_T. **d,** General pulse sequence, displaying the applied microwave pulses and detector readout pulses.

Figure 4 | Truth table amplitudes of the CNOT quantum gate. a, State counts (N_{00}, N_{01}, N_{10} and N_{11}) of the detectors after $n = 3$ CNOT rotations, for 8,192 single-shot measurements. **b,** Truth table amplitudes corrected for measurement visibility using conditional spectroscopy measurements. The average gate fidelity equals $F = 0.4$.

qualitatively agree with the amplitude matrix of an ideal CNOT gate:

$$M_{\mathrm{CNOT}} = \begin{pmatrix} 1 & 0 & 0 & 0 \\ 0 & 1 & 0 & 0 \\ 0 & 0 & 0 & 1 \\ 0 & 0 & 1 & 0 \end{pmatrix} \qquad (3)$$

The input states 0_C0_T and 0_C1_T remain unaffected by the gate and translate directly to the same output state, hence the two high values on the diagonal of the matrix. For the states 1_C0_T and 1_C1_T, the gate inverts the target qubit, explaining the two high off-diagonal values. Figure 4a can be related to Fig. 3 by considering the points at the intersections of the dotted lines of the latter. Note that the states 0_C and 1_C correspond to the elements from Fig. 3 where a 2π and 3π rotation, respectively, were induced, which explains the comparable input state fidelities.

The major factors contributing to the deviations of Fig. 4a from the ideal transfer matrix M_{CNOT} are qubit decoherence, control errors and measurement visibility. The last is only 40% for this sample; note that more advanced SQUID detection methods have approached 90% visibility[16]. To compensate for this influence, we performed conditional spectroscopy measurements[17] that convert the normalized detector counts P_{ij} to qubit state occupation probabilities. For an ideal single-shot detector, these two sets are identical. As explained in Supplementary Information, conditional spectroscopy provides two detection mechanisms in parallel for the control qubit: one using the control qubit detector directly and a second using the excitation spectrum of the target qubit. The latter is now used as a means to calibrate the former, in this way compensating for the effect of the limited measurement visibility. Using this technique, the CNOT data of Fig. 4a are corrected, and the result is depicted in Fig. 4b. Note that the influences of decoherence and control errors are preserved. We quantify the resulting average of the logical basis amplitude fidelities by $F = \mathrm{Tr}(M_{\mathrm{exp}} M_{\mathrm{CNOT}}^{\mathrm{T}})/4$, with $F = 1$ for the ideal case. The experimental data from Fig. 4b can be represented by the matrix M_{exp}:

$$M_{\mathrm{exp}} = \begin{pmatrix} 0.51 & 0.22 & 0.13 & 0.14 \\ 0.28 & 0.47 & 0.21 & 0.04 \\ 0.08 & 0.23 & 0.05 & 0.64 \\ 0.20 & 0.14 & 0.51 & 0.15 \end{pmatrix} \qquad (4)$$

resulting in $F = 0.4$. The significant reduction of F is mostly due to the short coherence time of this particular sample. We expect to increase this number to gate performances similar to that of simple microwave-driven Rabi experiments[6,16].

In order to use this gate in a quantum algorithm, the phase factors of the amplitudes of M_{exp} at the positions of non-zero elements of

M_{CNOT} have to be determined. Using a Ramsey-like interference experiment on n consecutive CNOT gates, we show that these phase shifts agree with the driven Rabi evolution. Equation (2) predicts that for $n = 2$ CNOT gates (that is, $\omega\tau = 2\pi$) a PHASE gate is executed which inverts the phase of the states 1_C0_T and 1_C1_T relative to the states 0_C0_T and 0_C1_T. The scheme used to measure this shift is depicted in Fig. 5b. First a $\frac{1}{2}\pi$ pulse with a fixed microwave phase is applied, bringing the control qubit into an equal weight superposition of states 0_C and 1_C. Next the CNOT gates are executed. The states before and after the gates are then interfered by means of a second $\frac{1}{2}\pi$ probe pulse, of which the microwave phase φ, corresponding to the rotation axis, is varied. In Fig. 5a the extra quantum phase between the states 0_C0_T and 1_C0_T is depicted. As expected, the Ramsey fringe is inverted by the quantum phase shift of $180°$ induced by a full Rabi cycle, thus executing a PHASE gate. Experimentally we find, in addition to the quantum phase, a second shift which is due to
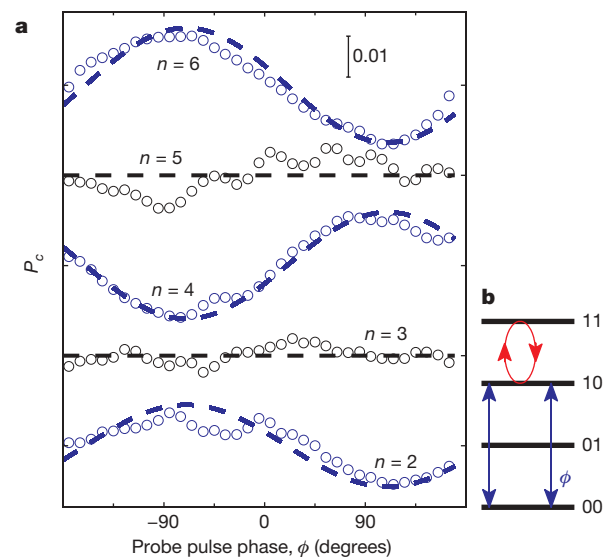

Figure 5 | Quantum phase induced after $n = 2$–6 CNOT operations. a, Phase probing of the control qubit with the relative microwave phase of the second Ramsey $\frac{1}{2}\pi$ pulse along the horizontal axis. After an odd number n of CNOT gates, the system population is in an entangled superposition of the states 0_C0_T and 1_C1_T (Bell state), extinguishing the Ramsey interference pattern. An even number of gates executes $n/2$ PHASE gates, and returns the system to a disentangled state, restoring the Ramsey signal. The $180°$ phase shift that occurs between even traces with $\Delta n = 2$ agrees with the description of driven Rabi evolution. **b,** The sequence of operations used to acquire the quantum phase shift of the CNOT gates.

off-resonant effects of the CNOT microwave pulse on the control qubit transition. It is distinguished from the quantum phase by performing a second measurement with exactly the same pulse sequence with the target qubit detuned from any relevant frequency. In this case, the CNOT gate pulse only induces the off-resonant z-rotation of the control qubit. We find that this effect is nearly linear in driving power and it is compensated for in Fig. 5a, leaving only the genuine quantum phase shift.

In conclusion, we have implemented the complete set of four two-qubit CNOT gates in a symmetric pair of superconducting flux qubits. Complemented with longer coherence times[6,16] and optimized detector visibility[16], the presented gates enable experiments on two-qubit quantum algorithms and solid-state qubit entanglement using the four Bell states. This scheme, combined with controllable coupling[12], forms an attractive and generic approach to the implementation of solid-state quantum computing.

1. Nielsen, M. A. & Chuang, I. L. *Quantum Computation and Quantum Information* (Cambridge Univ. Press, Cambridge, 2000).
2. Yamamoto, T., Pashkin, Yu. A., Astafiev, O., Nakamura, Y. & Tsai, J. S. Demonstration of conditional gate operation using superconducting charge qubits. *Nature* **425**, 941–944 (2003).
3. Steffen, M. *et al.* Measurement of the entanglement of two superconducting qubits via state tomography. *Science* **313**, 1423–1425 (2006).
4. Nakamura, Y., Pashkin, Yu. A. & Tsai, J. S. Coherent control of macroscopic quantum states in a single-Cooper-pair box. *Nature* **398**, 786–788 (1999).
5. Vion, D. *et al.* Manipulating the quantum state of an electrical circuit. *Science* **296**, 886–889 (2002).
6. Chiorescu, I., Nakamura, Y., Harmans, C. J. P. M. & Mooij, J. E. Coherent quantum dynamics of a superconducting flux qubit. *Science* **299**, 1869–1871 (2003).
7. Martinis, J. M., Nam, S., Aumentado, J. & Urbina, C. Rabi oscillations in a large Josephson-junction qubit. *Phys. Rev. Lett.* **89**, 117901 (2002).
8. Mooij, J. E. *et al.* Josephson persistent current qubit. *Science* **285**, 1036–1039 (1999).
9. Berkley, A. J. *et al.* Entangled macroscopic quantum states in two superconducting qubits. *Science* **300**, 1548–1550 (2003).
10. Majer, J. B., Paauw, F. G., Ter Haar, A. C. J., Harmans, C. J. P. M. & Mooij, J. E. Spectroscopy on two coupled superconducting flux qubits. *Phys. Rev. Lett.* **94**, 090501 (2005).
11. Grajcar, M. *et al.* Four-qubit device with mixed couplings. *Phys. Rev. Lett.* **96**, 047006 (2006).
12. Hime, T. *et al.* Solid-state qubits with current-controlled coupling. *Science* **314**, 1427–1429 (2006).
13. Pashkin, Yu. A. *et al.* Quantum oscillations in two coupled charge qubits. *Nature* **421**, 823–826 (2003).
14. McDermott, R. *et al.* Simultaneous state measurement of coupled Josephson phase qubits. *Science* **307**, 1299–1302 (2005).
15. Cory, D. G., Price, M. D. & Havel, T. F. Nuclear magnetic resonance spectroscopy: An experimentally accessible paradigm for quantum computing. *Physica D* **120**, 82–101 (1998).
16. Lupaşcu, A. *et al.* Quantum non-demolition measurement of a superconducting two-level system. *Nature Phys.* **3**, 119–125 (2007).
17. Ter Haar, A. C. J. *Single and Coupled Josephson Junction Quantum Bits.* PhD thesis, Delft Univ. Technology (2005).
18. Majer, J. B., Butcher, J. R. & Mooij, J. E. Simple phase bias for superconducting circuits. *Appl. Phys. Lett.* **80**, 3638–3640 (2002).